INFRASOUND AS A DEPTH DISCRIMINANT

Stephen J. Arrowsmith, Rod W. Whitaker, and Richard J. Stead

Los Alamos National Laboratory

Sponsored by the National Nuclear Security Administration

Award No. DE-AC52-06NA25396/LA09-Depth-NDD02

ABSTRACT

There is a need for routine measurements of infrasound from earthquakes, in conjunction with modeling, to better constrain our understanding of the generation of infrasound from earthquakes, in particular the effect of source depth. Here, we first outline a systematic search for infrasound from earthquakes from a range of magnitudes. Based on our observations, earthquakes with Mw>~5 appear to be reliable sources of infrasound, independent of depth, with the detection of infrasound at regional distances largely driven by path and receiver effects. We identified clear infrasound detections from large earthquakes as deep as 123 km. In contrast, earthquakes with Mw<~4 are poor infrasound sources and are unlikely to be detected regionally. In particular, we note that there has yet to be a conclusive detection from an earthquake with Mw<3.0. Our results imply that magnitude, rather than depth, appears to be the dominant factor influencing the generation of infrasound from earthquakes. To understand these observations further, we have developed a coupled seismoacoustic modeling technique comprising a three-dimensional (3D) finite difference algorithm, Rayleigh integral, and time domain parabolic equation. By gluing these techniques together, we are modeling the generation and propagation of infrasound from earthquakes. The effect of depth on these simulations, with comparison to our observational dataset, is discussed.

Report Documentation Page

Form Approved
OMB No. 0704-0188

1. REPORT DATE	2. REPORT TYPE	3. DATES COVERED
SEP 2011		**00-00-2011 to 00-00-2011**

4. TITLE AND SUBTITLE	5a. CONTRACT NUMBER
Infrasound as a Depth Discriminant	5b. GRANT NUMBER
	5c. PROGRAM ELEMENT NUMBER
6. AUTHOR(S)	5d. PROJECT NUMBER
	5e. TASK NUMBER
	5f. WORK UNIT NUMBER
7. PERFORMING ORGANIZATION NAME(S) AND ADDRESS(ES) **Los Alamos National Laboratory,P.O. Box 1663 ,Los Alamos,NM,87545**	8. PERFORMING ORGANIZATION REPORT NUMBER
9. SPONSORING/MONITORING AGENCY NAME(S) AND ADDRESS(ES)	10. SPONSOR/MONITOR'S ACRONYM(S)
	11. SPONSOR/MONITOR'S REPORT NUMBER(S)

12. DISTRIBUTION/AVAILABILITY STATEMENT
Approved for public release; distribution unlimited

13. SUPPLEMENTARY NOTES
Published in the Proceedings of the 2011 Monitoring Research Review - Ground-Based Nuclear Explosion Monitoring Technologies, 13-15 September 2011, Tucson, AZ. Volume II. Sponsored by the Air Force Research Laboratory (AFRL) and the National Nuclear Security Administration (NNSA). U.S. Government or Federal Rights License

14. ABSTRACT
There is a need for routine measurements of infrasound from earthquakes, in conjunction with modeling, to better constrain our understanding of the generation of infrasound from earthquakes, in particular the effect of source depth. Here, we first outline a systematic search for infrasound from earthquakes from a range of magnitudes. Based on our observations, earthquakes with Mw>~5 appear to be reliable sources of infrasound, independent of depth with the detection of infrasound at regional distances largely driven by path and receiver effects. We identified clear infrasound detections from large earthquakes as deep as 123 km. In contrast, earthquakes with Mw<~4 are poor infrasound sources and are unlikely to be detected regionally. In particular, we note that there has yet to be a conclusive detection from an earthquake with Mw<3.0. Our results imply that magnitude, rather than depth, appears to be the dominant factor influencing the generation of infrasound from earthquakes. To understand these observations further, we have developed a coupled seismoacoustic modeling technique comprising a three-dimensional (3D) finite difference algorithm, Rayleigh integral, and time domain parabolic equation. By gluing these techniques together, we are modeling the generation and propagation of infrasound from earthquakes. The effect of depth on these simulations, with comparison to our observational dataset, is discussed.

15. SUBJECT TERMS

16. SECURITY CLASSIFICATION OF:			17. LIMITATION OF ABSTRACT	18. NUMBER OF PAGES	19a. NAME OF RESPONSIBLE PERSON
a. REPORT	b. ABSTRACT	c. THIS PAGE			
unclassified	**unclassified**	**unclassified**	**Same as Report (SAR)**	**11**	

OBJECTIVES

The goal of this research is to determine whether infrasound might be useful for separating shallow events from deep events and possibly providing some estimate of focal depth. Our findings address this question but also provide more-general insights into the generation of infrasound from earthquakes. By modeling the generation of infrasound from earthquakes using a coupled seismoacoustic numerical approach, we show that the infrasound amplitude should indeed scale with earthquake depth, with a linear relation between the log of the infrasonic amplitude and the log of the depth. However, these findings are not borne out in the data acquired during this project, which demonstrate a good relationship between earthquake magnitude and the amplitude, but no clear relationship with depth. These findings highlight the need for more infrasound measurements of earthquakes at different depths in order to uniquely separate the various source and path effects in the real data.

RESEARCH ACCOMPLISHED

Data Analysis

The development of an empirical dataset is well described in the previous MRR papers under this project and is therefore not discussed in detail here (Arrowsmith et al., 2010). The lack of adequate data has hampered this effort, and it has been necessary to revise our strategy from requiring multiple array detections for robust association to focusing on signals from large earthquakes recorded within 1 skip distance in order to maintain an adequate sampling. The final dataset is summarized in Figure 1, which shows that the ambient noise levels appear to drive whether or not we observe detections, with no clear correlation between the detectability and the focal depth. To explore these relationships further, Figure 2 shows a comparison between the seismic magnitude and predicted path loss for the five undetected earthquakes with root mean square (RMS) noise levels below the dashed line in Figure 1 and the detected events. This figure shows that the undetected earthquakes associated with low RMS background noise are less likely to be detected due to their smaller size and high predicted path loss.

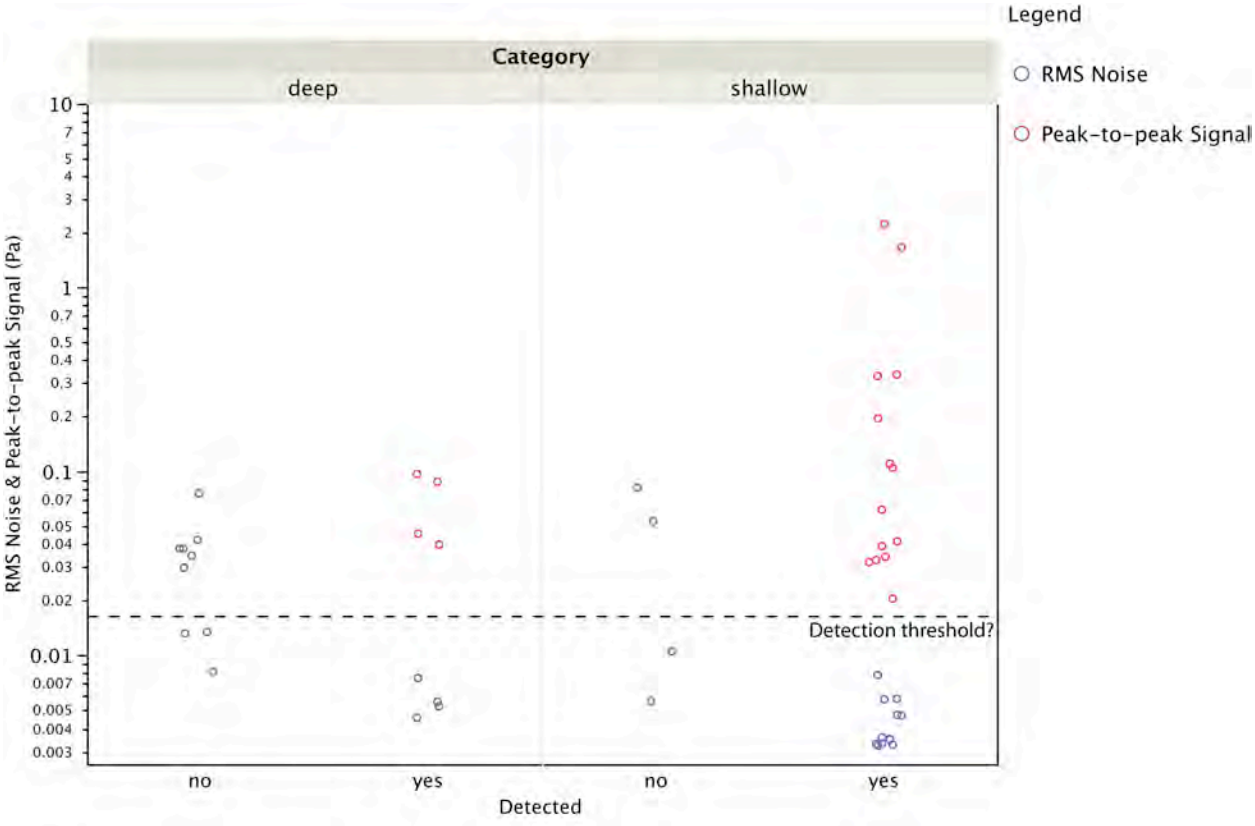

Figure 1. Summary of infrasonic detections from the earthquake dataset. An arbitrary threshold of 50 km is used to distinguish between "shallow" and "deep" earthquakes. Note that for detected events, both an RMS noise and peak-to-peak signal value are plotted; for undetected events, only an RMS noise value is plotted.

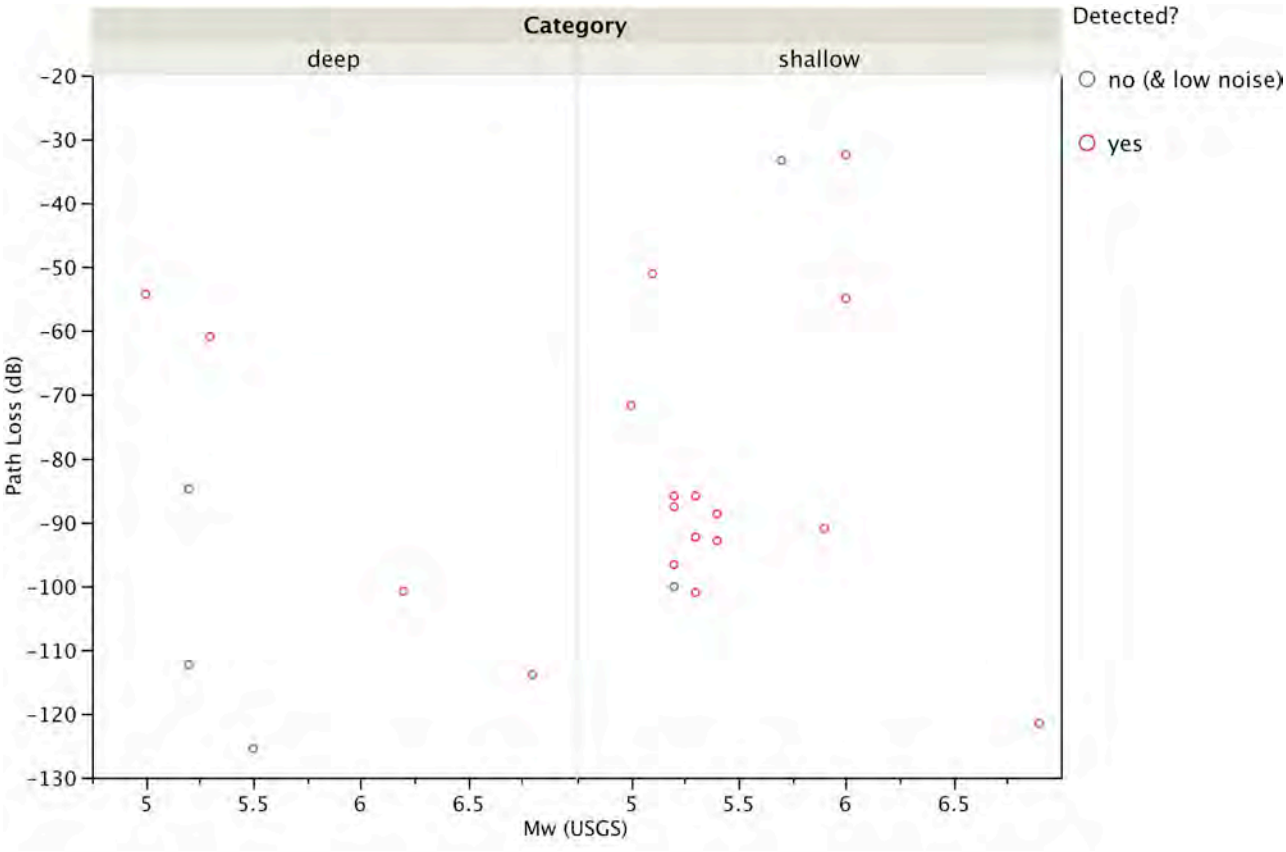

Figure 2. Comparison between undetected events with low noise (Figure 1) and detected events in terms of the seismic magnitude and predicted path loss from parabolic equation modeling. Four out of five of the undetected events have comparatively low magnitudes and high path loss—consistent with the lack of detection. However, one anomalous event has low path loss and a relatively high magnitude of 5.7.

For each detected earthquake, we have measured a variety of signal parameters using the beamformed, instrument-corrected trace. These parameters include the peak-to-peak amplitude in Pa, the period at maximum amplitude, the group velocity, the backazimuth deviation, and the cross-correlation coefficient.

The dominant frequency content of most of the infrasound signals is ~ 1 Hz. Spectra showing the detailed frequency content for four selected earthquakes are plotted in Figure 3. The spectra clearly show that, while the spectral content is indeed centered on ~ 1 Hz, the signals are typically in the range of ~0.5–3 Hz (although this varies somewhat from event to event). As shown in Figure 1, peak-to-peak signal amplitudes span two orders of magnitude from ~0.02 to 2 Pa. Ambient noise levels at the arrays suggest that the robust detection of signals below ~0.02 Pa is likely to be difficult (Figure 1). Azimuthal deviations have a standard deviation of 5.9°, broadly consistent with magnitudes of backazimuth deviations predicted over multiple years from ray tracing (Drob et al., 2010).

Modeling

We have developed a coupled numerical source model for modeling the generation of infrasound from earthquakes. The coupled model fuses a three-dimensional (3D) finite difference time domain code (ELAS3D—Larson and Shultz, 1995) with a Rayleigh integral code that we have developed. Acceleration time-histories are calculated on a 2D grid centered on the epicenter, providing the initial conditions for the Rayleigh integral calculation. As discussed in detail in Blackstock (2000), the Rayleigh integral can be used to calculate the acoustic pressure at some distance from a baffled piston (i.e., all acoustic radiation is constrained to propagate in the forward direction) as an integral of contributions from accelerations of all infinitesimal area elements, *dS*, of the piston:

$$p(x,y,z;t) = \rho_0 \int_S \frac{\dot{u}_p(x',y';t - R/c_0)}{2\pi R} dS,$$

where *x'*, *y'* are the coordinates of the source point on the piston, *R* is the distance to the field point of interest, ρ_0 is the air density, and c_0 is the speed of sound in air.

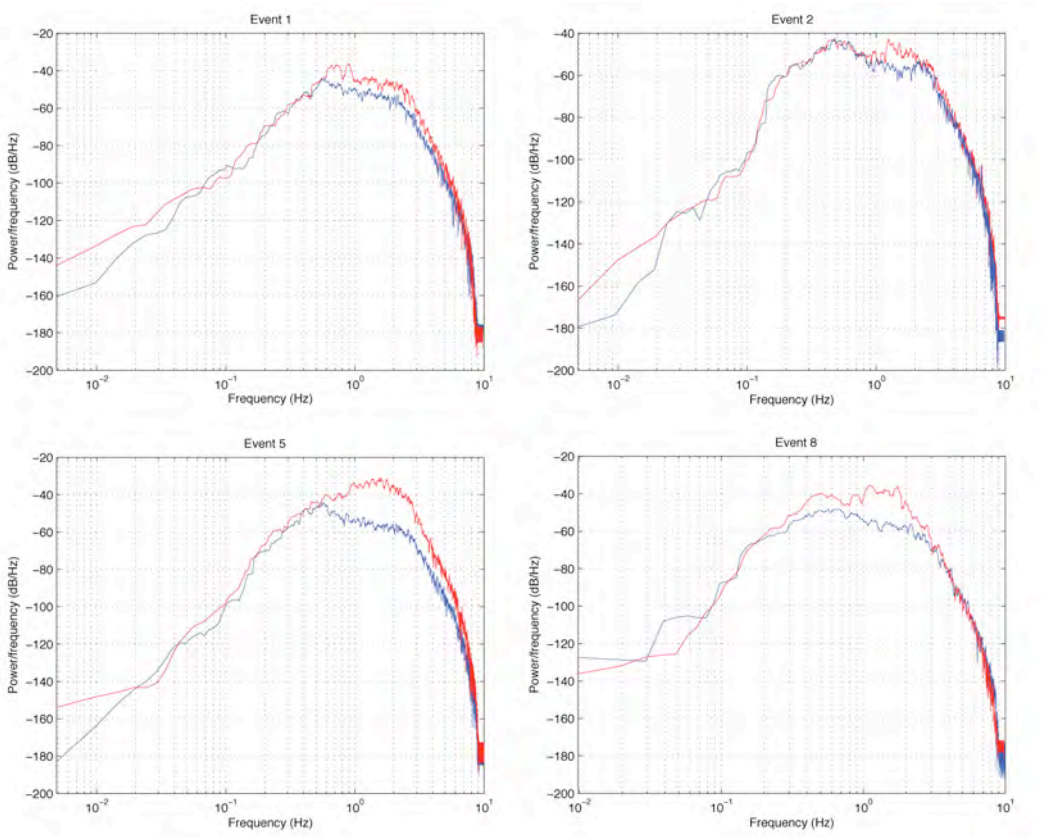

Figure 3. Spectra for infrasound signals (red curves) and corresponding pre-event noise (blue curves) for four different events. The top panel represents two relatively low seismic magnitude deep events, while the bottom panel represents two shallow earthquakes from Tanzania recorded at I32KE.

The Rayleigh integral is an approximation to the Helmholtz-Kirchoff integral theorem and is strictly valid in the far-field, beyond the Rayleigh distance, defined in general by

$$R_0 \equiv \frac{S}{\lambda},$$

where S is the surface area of the piston. This limitation imposes a constraint on the area of the piston that can be modeled, since the assumption of a constant sound speed, c_0, becomes unrealistic at large distances from the source due to the variation of temperature and winds with height. We have performed a series of synthetic calculations using different piston areas, and we find that the far-field approximation is appropriate at 5 km elevation from a 3×3 km^2 region (Figure 4). We choose this as an approximate limit on the size of the region that can be modeled.

The radiation pattern can be characterized by an amplitude directivity factor, D, which is defined as the pressure at any angle θ relative to that (at the same range r) at $\theta = 0$:

$$D(\theta) = \frac{P(r,\theta)}{P(r,0)}.$$

The radiation pattern from a circular piston of radius *a* can be calculated from (Blackstock, 2000)

$$D(\theta) = \frac{2J_1(ka\sin\theta)}{ka\sin\theta},$$

where J_1 is the first-order Bessel function of the first kind, *k* is the wavenumber $(k = 2\pi/\lambda)$, and θ is the angle from the zenith. The number of nulls and secondary maxima in the radiation pattern is determined by the size of *ka*. As the piston size increases, relative to the wavelength, the number of nulls increases.

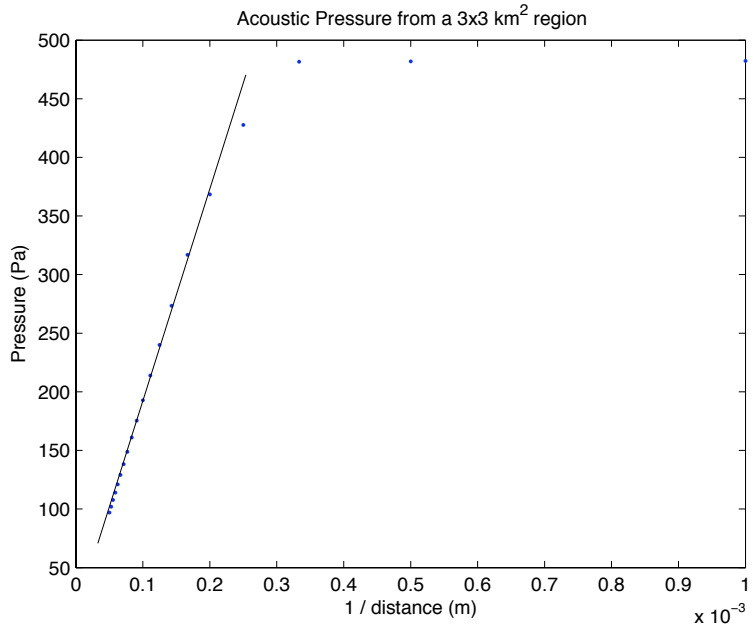

Figure 4. Acoustic pressure from a 3 × 3 km^2 region at different heights (1–20 km in increments of 1 km) assuming a constant acceleration of 1 m/s^2. Above 5 km, the predicted pressure falls off as 1/r, indicating that the far-field assumption is valid above this height.

The January 3, 2011, Circleville earthquake, which is discussed in further detail in Arrowsmith et al. (2011, this Proceedings) provides a good case study to explore the effect of earthquake depth on the recorded signals. Additional details on this event are available in Arrowsmith et al. (2011). Using the Harvard centriod moment tensor (CMT) solution, one-dimensional (1D) velocity model for southern Utah, and a Gaussian source time function of 1 s duration, we model the infrasound generated due to accelerations in the 3 × 3 km^2 region centered on the epicenter and calculate the associated radiation pattern at a frequency of 1 Hz (Figure 5). By performing ray-tracing using the G2S atmospheric model for this event, we find that the minimum launch angle required to produce a return for the source-receiver geometries is 52° from the zenith, corresponding to a maximum value of $D(\theta)$ equal to 0.005 (Figure 5). At the focal depth of 12 km, we estimate a source amplitude of 332.8 Pa on-axis, which equates to a maximum of 1.66 Pa at the source (332.8 × 0.005) that can be ducted. By scaling our synthetics accordingly, and using a time-domain parabolic equation (PE) method to estimate the resultant acoustic pressures at each receiver, we find remarkably good agreement (the average difference between observed and predicted pressure is 0.05 Pa). Having obtained confidence in this modeling approach, we explore the effect of depth on the near-field simulations, noting that these results are specific to a particular geology and source mechanism. The acoustic waveforms for four different simulations at depths of 5 km, 12 km (the Harvard CMT depth), 50 km, and 100 km (with all other

parameters held constant) are shown in Figure 6. The modeling predicts that there should be a clear relationship between earthquake depth and the near-field infrasound amplitude (Figure 7). Of course, the actual amplitudes detected in the far-field would be reduced by directivity and path effects, but this factor would be constant assuming the same time and source-receiver geometry.

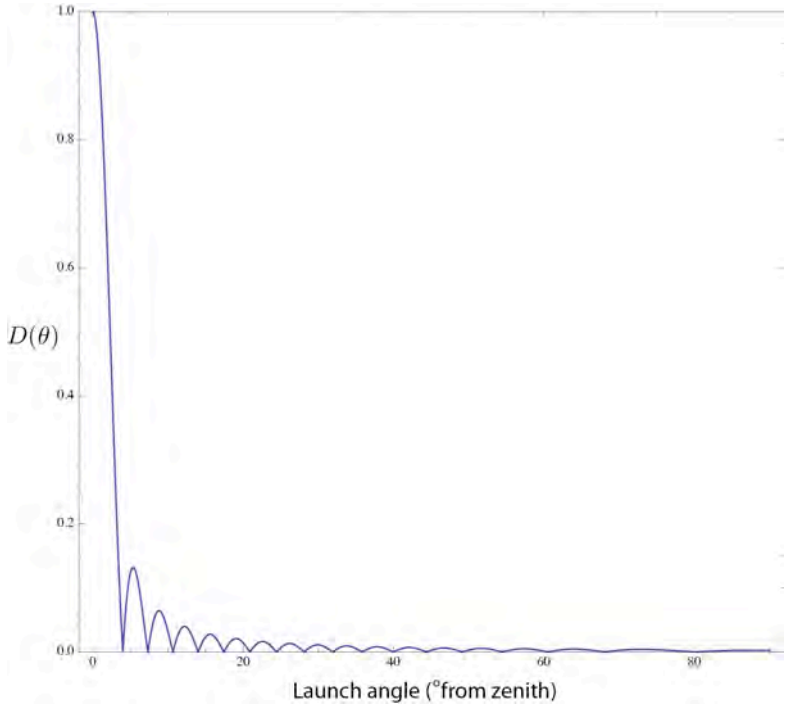

Figure 5. Radiation pattern for the piston modeled for the Circleville earthquake at a frequency of 1 Hz (wavelength of 340 m).

Scaling Laws

The development of an empirical relationship between event depth and the far-field infrasound amplitude requires some correction for the effect of path on the reduction of infrasound amplitudes. Here, we explore two techniques for performing path corrections. The first technique is based on an empirical formula derived from observations of underground nuclear tests by Mutschlecner et al. (1999) and provides an amplitude, A_n, normalized for distance and stratospheric wind speeds:

$$A_n = A_0 10^{-kV_d} \left(\frac{R}{R_s} \right)^S ,$$

where s =1.45, k =0.018 s/m, R is the great circle distance to the epicenter, R_s is an arbitrary standard distance, and v_d is the stratospheric wind component directed from source to array.

The second technique uses a PE model (West et al., 1992) to predict path losses due to both geometric spreading and absorption from source to receiver. The PE model can predict a path-loss in dB relative to 1 km, which can subsequently be used to scale all recorded amplitudes to 1 km from

$$P_{1\,\mathrm{km}} = \frac{P_{\mathrm{rec}}}{10^{\left(\frac{A}{20}\right)}} .$$

Mutschlecner et al. (1999) did not have access to modern four-dimensional atmospheric models such as the ground-to-space (G2S) model; thus, we intend to determine whether the second technique might reduce the variance in earthquake scaling laws. One notable difference between the two techniques is that the PE method can be applied to any phase, whereas the Mutschlecner et al. (1999) method is strictly for stratospheric returns.

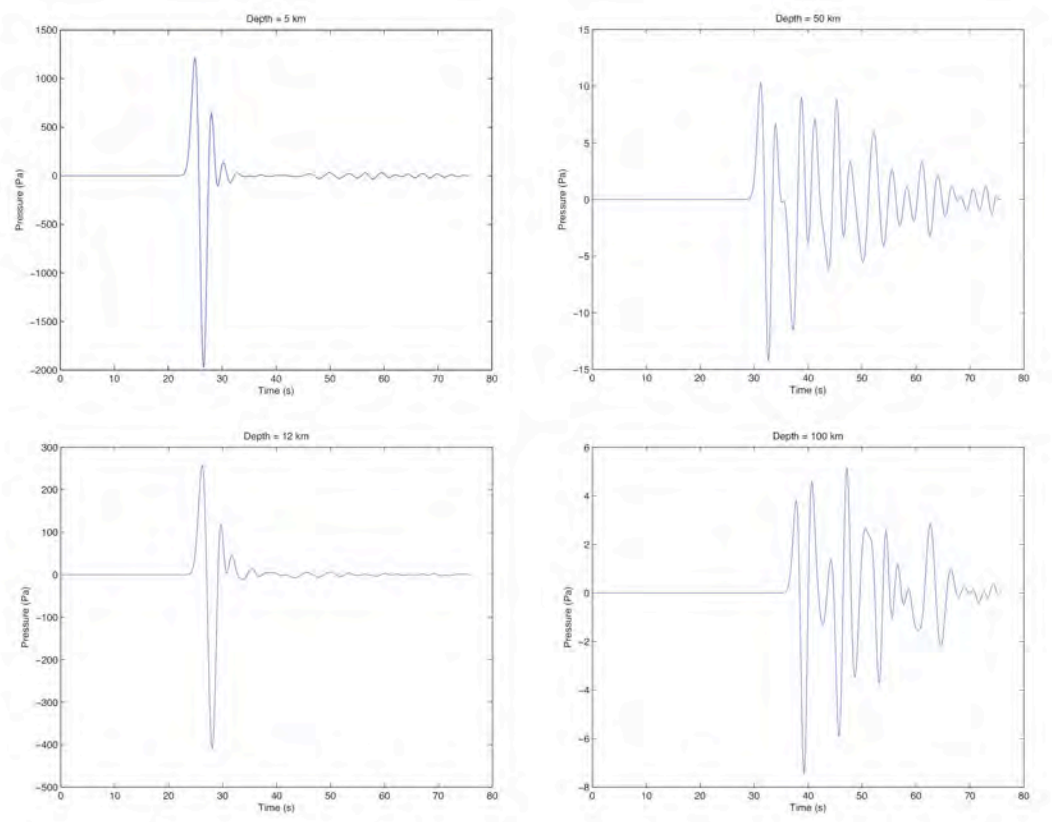

Figure 6. Simulated on-axis near-field infrasound waveforms at 5 km above the earthquake epicenter from an earthquake at 5 km depth (top left), 12 km depth (bottom left), 50 km depth (top right), and 100 km depth (bottom right).

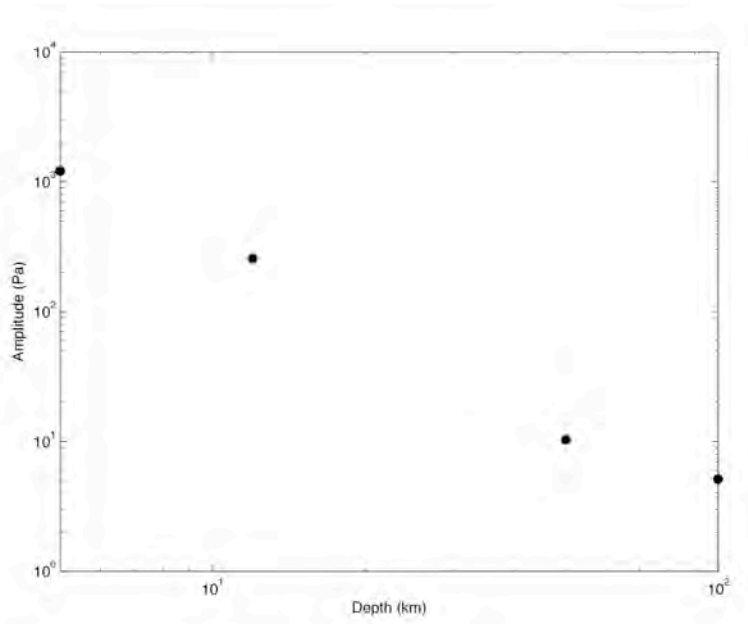

Figure 7. Relationship between focal depth and the peak modeled near-field on-axis infrasonic amplitude for the January 3, 2011, Circleville earthquake (the actual earthquake focal depth was ~12 km).

Following Mutschlecner and Whitaker (2005) and Le Pichon et al. (2006), we expect to obtain a linear relationship between magnitude and the log of the amplitude (corrected for path effects). Our results (Figure 8) show that indeed there is such a relationship, albeit with a relatively low correlation. The correlation reduces somewhat after correcting for path effects using PE modeling (i.e., reducing all amplitudes to 1 km), but there is still some large variability that remains unaccounted for. Using the Mutschlecner et al. (1999) path correction, and excluding arrivals with celerities outside the stratospheric range of 0.28–0.31 km/s, we obtain a much better fit ($R^2 = 0.65$), albeit with fewer data points. The regression obtained is similar to the Mutschlecner and Whitaker (2005) regression, which used M_L instead of Mw:

$$\log(A_n) = 0.70 M_W - 5.96.$$

Our initial hypothesis to test was that the scatter in the plots in Figure 8 could be explained by differences in event depth. However, plotting the residuals from the regression against depth (Figure 9) shows that there is no clear relationship with depth. Clearly, one issue is that the seismically obtained depths are themselves poorly constrained. However, one can think of the events as being robustly separated into two well-constrained populations—deep and shallow. As shown in Figure 9, there is no separation between the two populations.

A Brief Discussion of Small Earthquakes

This paper has focused on the study of large earthquakes with Mw>5.0. A complementary study discussed in Arrowsmith et al. (2011, this Proceedings) focuses on small earthquakes, which appear to be relatively poor infrasound sources. At low magnitudes (Mw<4.0), we find that—in comparison with manmade surface explosions of equivalent seismic magnitude—earthquakes are rarely detected at regional distances. This point is highlighted here because it suggests that the use of infrasound as a source-type discriminant may be of more practical value in the near-term than the use of infrasound as a depth discriminant.

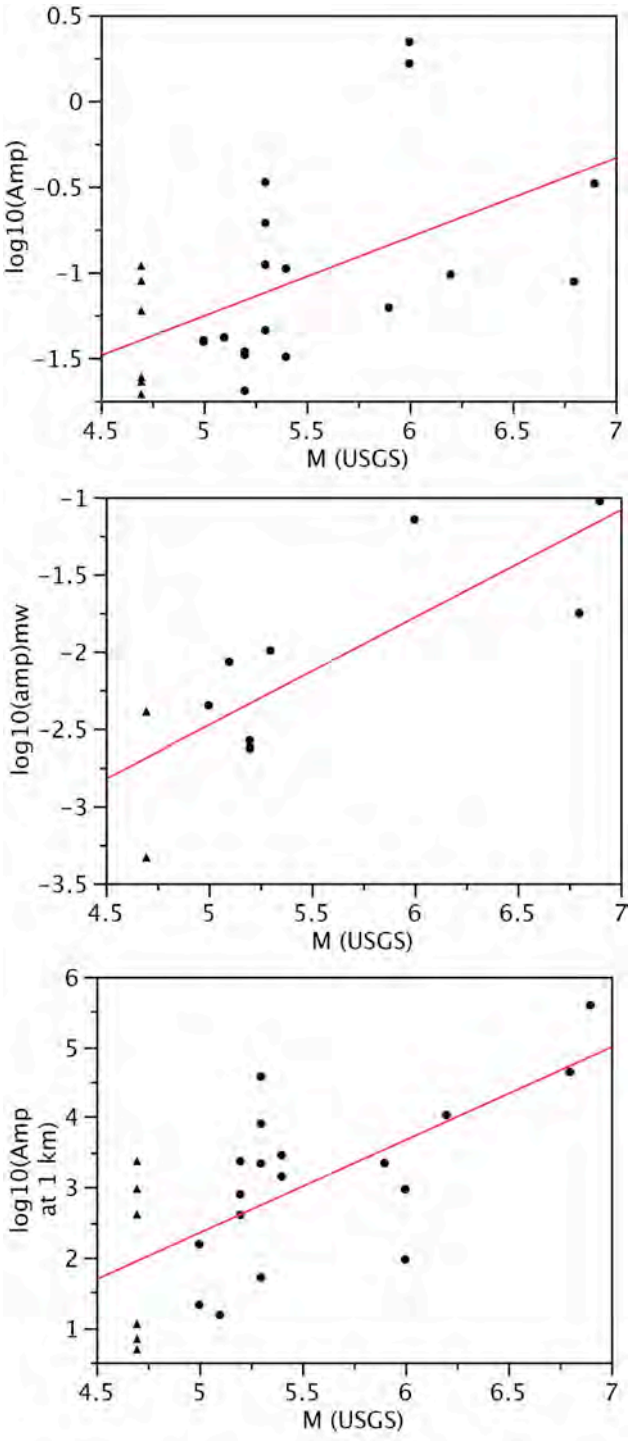

Figure 8. Graphs showing the relationship between the raw peak-to-peak amplitude and Mw (top panel), the peak-to-peak amplitude with the Mutschlecner et al. (1999) stratospheric wind correction, for signals with stratospheric celerities only (center panel) and the peak-to-peak amplitude—corrected for path loss—and Mw (bottom panel). We note that similar plots were obtained for our measurements of RMS amplitudes that were evaluated in 10 s windows centered on the peak amplitude. Black triangles depict measurements of signals from the 2011 Circleville, Utah, earthquake. The red lines on each plot denote the best least squares fit, which is best after applying the Mutschlecner and Whitaker correction (R^2 = 0.65).

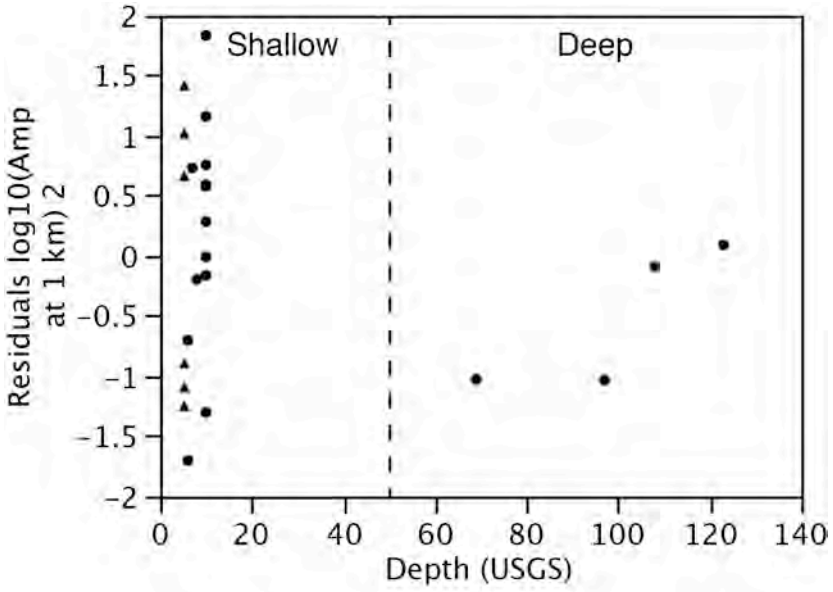

Figure 9. Relationship between residuals from the regression shown in Figure 8 (lower panel) and the depth obtained from the United States Geological Survey (USGS) earthquake catalog. Although seismic depths may be poorly constrained, the separation between shallow (< 50 km) and deep (> 50 km) should be robust. Black triangles depict measurements of signals from the 2011 Circleville, Utah, earthquake.

CONCLUSIONS AND RECOMMENDATIONS

- We have developed a numerical approach for modeling the generation of infrasound from earthquakes and show that for the January 3 Circleville, Utah, earthquake, the predicted amplitudes are consistent with the observations.
- Numerical modeling of the generation of infrasound from earthquakes predicts a linear relationship between the log of the infrasound amplitude and the log of depth.
- Empirical analysis confirms that infrasound amplitude scales with magnitude—as previously confirmed by Mutschlecner and Whitaker (2005) and Le Pichon et al. (2006)—but indicates that depth either plays no significant role or else is obscured by other effects that have not been accounted for (in contrast to the modeling).
- The Mutschlecner et al. (1999) path correction appears to be more robust for predicting path corrections than is PE modeling.
- Future research is recommended in the following areas: (1) continued dataset development, (2) improvements to source modeling (Kirchoff-Helmholtz), and (3) improvements to path corrections.

ACKNOWLEDGEMENTS

We thank Hans Hartse, Dale Anderson, Steve Taylor, and George Randall for their contributions at various phases of this research. We also acknowledge our ongoing interactions with the University of Utah and Southern Methodist University on a BAA project, which has provided some of the data used for this project.

REFERENCES

Arrowsmith, S. J., M. Hale, R. Burlacu, K. L. Pankow, B. W. Stump, C. Hayward, G. E. Randall, and S. R. Taylor (2011). Infrasound signal characteristics from small earthquakes, these Proceedings.

Arrowsmith, S., H. Hartse, S. Taylor, R. Stead, and R. Whitaker (2010). Infrasound as a depth discriminant, in *Proceedings of the 2010 Monitoring Research Review: Ground-Based Nuclear Explosion Monitoring Technologies*, Vol. 11, pp. 657–666.

Blackstock, D. T. (2000). *Fundamentals of Physical Acoustics*, Wiley-Interscience, New York.

Drob, D. P., M. Garces, M. A. H. Hedlin, and N. Brachet (2010). The temporal morphology of infrasound propagation, *Pure appl. geophys.*, doi:10.1007/s00024-010-0080-6

Larsen, S. and C. A. Schultz (1995). ELAS3D: 2D/3D elastic finite-difference wave propagation code, Lawrence Livermore National Laboratory technical report UCRL-MA-121792.

Le Pichon, A., P. Mialle, J. Guilbert, and J. Vergoz (2006). Multistation infrasonic observations of the Chilean earthquake of 2005 June 13, *Geophys. J. Int.* 167: 838–844.

Mutschlecner, J. P., R. W. Whitaker, and L. H. Auer (1999). An empirical study of infrasound propagation, Los Alamos National Laboratory report LA-13620-MS.

Mutschlecner, J. P. and R. W. Whitaker (2005). Infrasound from earthquakes, *J. Geophys. Res*. 110: doi:10.1029/2004JD005067.

West, M., K. E. Gilbert, and R. A. Sack (1992), A tutorial on the parabolic equation (PE) model used for long range sound propagation in the atmosphere, *Applied Acoustics* 37: 31–49.